

Characterization of photoinduced normal state through charge density wave in superconducting $\text{YBa}_2\text{Cu}_3\text{O}_{6.67}$

H. Jang,^{1,2,†} S. Song,^{3,†} T. Kihara,⁴ Y. Liu,⁵ S.-J. Lee,⁵ S.-Y. Park,¹ M. Kim,¹ H.-D. Kim,¹ G. Coslovich,³ S. Nakata,⁶ Y. Kubota,^{7,8} I. Inoue,⁷ K. Tamasaku,⁷ M. Yabashi,^{7,8} H. Lee,⁹ C. Song,^{2,9} H. Nojiri,⁴ B. Keimer,⁶ C.-C. Kao,¹⁰ and J.-S. Lee^{5,*}

¹PAL-XFEL, Pohang Accelerator Laboratory, Pohang, Gyeongbuk 37673, Republic of Korea

²Photon Science Center, Pohang University of Science and Technology, Pohang, Gyeongbuk 37673, Republic of Korea

³Linac Coherent Light Source, SLAC National Accelerator Laboratory, Menlo Park, California 94025, USA

⁴Institute for Materials Research, Tohoku University, Katahira 2-1-1, Sendai, 980-8577, Japan

⁵Stanford Synchrotron Radiation Lightsource, SLAC National Accelerator Laboratory, Menlo Park, California 94025, USA

⁶Max Planck Institute for Solid State Research, Heisenbergstr. 1, 70569 Stuttgart, Germany

⁷RIKEN SPring-8 Center, Sayo, Hyogo 679-5148, Japan

⁸Japan Synchrotron Radiation Research Institute, Sayo, Hyogo, 679-5198, Japan

⁹Departments of Physics, Pohang University of Science and Technology, Pohang, Gyeongbuk 37673, Republic of Korea

¹⁰SLAC National Accelerator Laboratory, Menlo Park, California 94025, USA

[†]These authors contributed equally to this work.

*Correspondence to: jslee@slac.stanford.edu (Jun-Sik Lee)

The normal state of high- T_c cuprates has been considered one of the essential topics in high-temperature superconductivity research. However, compared to the high magnetic-fields study of it, understanding a photoinduced normal state remains elusive. Here, we explore a photoinduced normal state of $\text{YBa}_2\text{Cu}_3\text{O}_{6.67}$ (YBCO) through a charge density wave (CDW) with time-resolved resonant soft x-ray scattering, as well as a high-magnetic field x-ray scattering. In the non-equilibrium state in which people predict a quenched superconducting state based on the previous optical spectroscopies, we experimentally observed a similar analogy to the competition between superconductivity and CDW shown in the equilibrium state. We further observe that the broken pairing states in the superconducting CuO_2 plane via the optical pump lead to nucleation of three-dimensional CDW precursor correlation, revealing that the photoinduced CDW is similar to phenomena shown under magnetic fields. Ultimately, these findings provide a critical clue that the characteristics of the photoinduced normal state show a solid resemblance to those under magnetic fields in equilibrium conditions.

Introduction

High- T_c cuprate is one of the most studied systems in strongly correlated materials since the first discovery of high-temperature superconductivity (HTSC) was reported in 1986 (1). Despite this high level of focus, a fundamental mechanism of HTSC is unclear because of many conundrums (2–4). Even with the tremendous research efforts in this field, realizing room-temperature superconductivity under the ambient pressure remains a huge challenge. Meanwhile, it has been considered that understanding the normal states of high- T_c cuprates and their corresponding features, e.g., pseudogap (5,6) and charge density wave (CDW) (7–20), could shed light on a direction to approach room temperature superconductivity. In this regard, an in-depth study on the ground state of the normal state is of profound significance to HTSC research.

An experimental study on the ground state problem is generally accompanied by the cooling of samples because they should be at the lowest possible energy state. In the HTSC case, due to the emergence of superconductivity (SC) below T_c , however, it is difficult to resolve the normal state at low temperature. Typically, this difficulty is overcome by quenching the superconducting state at low temperature by an external magnetic field (21–30). For example, x-ray scattering studies

on $\text{YBa}_2\text{Cu}_3\text{O}_{6+\delta}$ cuprates under high-magnetic fields revealed that the three-dimensional (3D) CDW correlation is the ideal ordering state in the normal state (24–30). Meanwhile, quenching the SC through the optical pump is considered another approach and has been demonstrated in many cuprates (31–39). However, a study on corresponding a normal state triggered by the laser-driven quench of the superconducting state is still in the early stage, although a photoinduced CDW state was recently reported on $\text{YBa}_2\text{Cu}_3\text{O}_{6+\delta}$ (40). In addition, findings through the pump-probe approach and corresponding implications represent fundamental physics of the non-equilibrium state, while the magnetic field study secures the equilibrium state. In this manner, despite that these two approaches' successful implementations in many high- T_c cuprates, it is still premature to reach a common ground on the normal state studied through those two approaches. Hence, it is timely to establish a scientific connection between the equilibrium state and the non-equilibrium state in HTSC.

Here we explore a photoinduced normal state of ortho-VIII $\text{YBa}_2\text{Cu}_3\text{O}_{6.67}$ (YBCO) by using a time-resolved resonant soft x-ray scattering (tr-RSXS) study and also carry out a pulsed high magnet field x-ray scattering experiment (see Methods). For this purpose, we focus on investigating CDW phenomena of YBCO while the superconducting state is quenched by the optical pump. This is because we are motivated by the fact that the CDW correlation is a normal state phenomenon (3,4) and has ubiquitously been established in high- T_c cuprates (7–20). In particular, there exists previous extensive previous studies, even with magnetic fields, on the CDW phenomena in $\text{YBa}_2\text{Cu}_3\text{O}_{6+\delta}$ cuprates (12–14,24–30,40). Thus, it allows us to compare this study to the CDW phenomena measured with the magnetic field, leading to an in-depth insight into the connection between the equilibrium and non-equilibrium states in the high- T_c cuprates. Moreover, there is no systematic experimental study regarding intertwined phenomena between the photoinduced CDW and the quenched SC state. In this study, we directly observe that both intensity and correlation length of the CDW order in YBCO are enhanced while the optical pump suppresses the superconducting state, indicating that the competition between CDW and SC shows a strong resemblance to that under those magnetic fields (13,24–30). It is also worthwhile to note that we basically assume a quench of the SC state through the previous optical demonstrations (31–39). We further observe an emergence of a three-dimensional CDW precursor correlation (27) under the photoinduced normal state of YBCO. From these findings,

we bring up a point that CDW phenomena in the equilibrium state are characteristically identical to those in the non-equilibrium state. In addition, we suggest that the broken Cooper-pairing physics could be discussed in the context of the nucleation of the vortex state through the external magnetic field. Inversely, it allows us to extend our scientific consideration even under the equilibrium state into the fact that the non-equilibrium approach could generate a transient superconducting state nearly up to room temperature (41–44).

Results

CDW of ortho-VIII $\text{YBa}_2\text{Cu}_3\text{O}_{6.67}$ under the equilibrium state. One of the profound discoveries in high-Tc cuprates is the universal existence of a static CDW (or charge order) in CuO_2 planes (7–20). In the underdoped $\text{YBa}_2\text{Cu}_3\text{O}_{6+\delta}$ cuprates, a CDW typically appears in the pseudogap phase (12–14,24–30). In other words, the onset temperature of CDW (T_{cdw}) exists in the normal state. Many researchers believe its ground state is critical to understand the superconducting behavior in $\text{YBa}_2\text{Cu}_3\text{O}_{6+\delta}$ (3,28).

Figure 1A shows a temperature dependence of static CDW of the YBCO crystal, which was measured by resonant soft x-ray scattering (RSXS) measurement (see Methods). We observed CDW peaks at $Q = (0, q_{\text{cdw}}, \sim 1.45)$ where q_{cdw} is around -0.32 reciprocal lattice unit (r.l.u.) in the CuO_2 plane (fig. S1). The CDW appears below ~ 150 K, which is consistent with previous studies (24–27). As expected, the CDW, which is developed from the normal state, is suppressed while the superconducting state emerges below $T_c = 65.5$ K. This suppression demonstrates the existence of competition between CDW and SC in YBCO, as shown in other $\text{YBa}_2\text{Cu}_3\text{O}_{6+\delta}$ cuprates (12–14,24–30). At the same time, it reveals that a study of CDW's ground state at low temperature (i.e., the normal state) is challenging because of the coexistence of SC and its competition with the CDW. Hence, to investigate a low-temperature state of CDW, the SC needs to be quenched. As a magnetic field causes a vortex state (i.e., quenched SC state), an optical pump can also break Cooper pairs in superconducting CuO_2 planes (31–40) when the pumping conditions are appropriately tuned (see Fig. 1B).

CDW of YBCO under the non-equilibrium state. Figure 2A shows an experimental configuration of tr-RSXS, aiming to explore CDW phenomena of YBCO at low temperatures.

We used a 1.55 eV (800 nm) optical laser with a fluence of $15 \mu\text{J}/\text{cm}^2$ (see Methods), aimed to minimize thermal heating (Supplementary). Figure 2B shows the temporal behavior of the CDW order at $T = 25 \text{ K}$, which was measured at $Q = (0, -0.32, 1.45)$. Before the pump – i.e., time delay (Δt) < 0 , it shows a persistent CDW signal suppressed by the competition with SC. After the pump, we observed an enhancement of the CDW for $0 < \Delta t < \sim 7 \text{ ps}$, which is consistent with the previous work (40). For the $0 < \Delta t < 0.5 \text{ ps}$ range, the CDW suppression is associated by a photoexcited charge-carrier while SC is suppressed (see Fig. S6) (35). Also, the maximum enhancement of the CDW occurs at $\Delta t \sim +0.9 \text{ ps}$. Figure 2C shows the CDW peak profiles at $\Delta t < 0$ and $\Delta t = +0.9 \text{ ps}$. The photoinduced CDW peak at $\Delta t = +0.9 \text{ ps}$ becomes stronger and sharper than that at the negative time delay ($\Delta t = -1.1 \text{ ps}$). This implies that the CDW volume fraction in CuO_2 planes at the pumped moment is recovered from that suppressed by the SC.

In order to scrutinize the photoinduced phenomena, we explored the temperature dependence of CDW scanned at $Q = (0, k, \sim 1.45)$. Figure 3A shows the CDW peak profiles measured at both $\Delta t = -1.1 \text{ ps}$ and $+0.9 \text{ ps}$ with different sample temperatures. Note that full delay scans are in fig. S2. Below T_c , the photoinduced behavior becomes more pronounced. This indicates the CDW enhancement behavior is associated with the quenched SC state. For more quantitative analysis, we fitted both peak profiles and plotted a summary [CDW area (i.e., integrated intensity), peak width, and area difference] in Fig. 3B. The enhanced CDW area clearly shows a contrast below T_c . The correlation length, $\xi = 2/\text{FWHM}$ (where FWHM is the full width at half maximum of the Lorentzian profile) of the photoinduced CDW peak at $T = 15 \text{ K}$ is estimated to be $\sim 88 \text{ \AA}$, which is about a 60 % increase compared to the case at $\Delta t = -1.1 \text{ ps}$. Under the scattering perspective, this deduces that the domain size of CDW becomes larger (i.e., its volume fraction) while SC's volume fraction could be suppressed by the pump. These findings show a strong resemblance to CDW phenomena under external magnetic fields (24–30). Moreover, the optically pumped CDW area is maximized at $T \sim 55 \text{ K}$. This indicates that the T_c under the optically pumped condition is shifted lower because the superconducting state needs more energy to form under this pumped condition, which is consistent with typical behavior of a superconductor under a magnetic field (22, 45–46). However, the photoinduced CDW peak measured at 65 K ($\sim T_c$) is slightly weaker ($\sim 17.7 \%$) than the CDW peak measured at $\Delta t = -1.1 \text{ ps}$. It means that optical pumping causes melting of not only SC in the CuO_2 planes but also some portion of the CDW regardless of the

existence of SC, like the case of pure CDW material (35). Nevertheless, it is possible to observe the photoinduced CDW behavior in YBCO because the temporal dynamics of CDW are slightly faster (about 100 fs) than that of SC (see fig. S4). Hence, the photoinduced CDW features observed at $\Delta t = +0.9$ ps could be attributed to a combined response from both the melted portion by optical pumping and recovered portion by photoinduced suppression of SC.

Three-dimensional CDW correlation in the photoinduced normal state of YBCO. Considering the temperature dependence on the photoinduced CDW behavior in YBCO, it is reasonable to find a crossover in CDW phenomena between the optical pump approach and the magnetic field (H) approach as a next step. This triggered us to explore a signature of the long-ranged three-dimensional (3D) CDW under the normal state that occurs when an H -field stronger than 50 % of H_{c2} is applied (27–29). In this sense, we performed L -dependence measurement of the CDW under the transient state, aiming to explore whether the optical pump also induces a 3D CDW behavior in YBCO.

Figure 4A shows CDW peak profiles at both $\Delta t = -1.1$ ps and $+0.9$ ps with different detector (2θ) angles (i.e., L -dependence) at $T = 25$ K. Note that details of this detector angle dependent measurement are in the Supplementary materials. At $\Delta t = -1.1$ ps, the CDW peak gets weaker when the l -value moves toward 1 r.l.u. (see summarized CDW peak heights in Fig. 4B), which reproduces the typical quasi-2D CDW behavior in $\text{YBa}_2\text{Cu}_3\text{O}_{6+\delta}$ cuprates that the CDW intensity is maximized around a half-integer ($l \sim 1.5$ r.l.u.) (12–14, 24–30). For $\Delta t = +0.9$ ps, we observed a different photoinduced behavior with varying 2θ (also see fig. S3). The photoinduced CDW behavior gets pronounced as the l -value decreases from ~ 1.45 to ~ 1.08 r.l.u. Nevertheless, no clear feature of a long-ranged 3D order was observed that would have been clearly visible in this YBCO under the high magnetic field (see Fig. 4C). However, as shown in Fig. 4B summary, we found an interesting tendency that the photoinduced CDW order is maximized at $l \sim 1.2$ r.l.u., which is close to an integer l -value. This L -dependence of the photoinduced CDW indicates a 3D CDW precursor correlation observed in high magnetic field measurements (27). It would also be worthwhile to note that the photoinduced state is still a mixture between the transient state and the reduced SC portion because of not reaching a full 3D CDW order.

According to the magnetic field experiments on $\text{YBa}_2\text{Cu}_3\text{O}_{6+\delta}$ cuprates (12–14,24–30), the development of the 3D CDW precursor suggests that the SC quenching effect via our optical pump condition is equivalent to that of the external magnetic field effect of between $H = 10$ and 14 T. Note that this field estimation is the simplest scaling analysis based on the assumption that the primary mechanism of CDW formation is electronic (see fig. S8). Although the lattice is always strongly coupled to an electron and somewhat affects the dynamics when an optical pump induces a thermal effect, the photoinduced CDW order's L -dependence (Fig. 4B and fig. S3), which cannot be explained by the lattice change, supports that the thermal heating is not dominant in this case. In this regard, the T_c shift shown in Fig. 3 is also interpreted to correspond to the equilibrium state under the estimated magnetic field (24,25). Furthermore, considering some portion of the CDW in the CuO_2 planes melted by the optical pump, the practical CDW portion in the optical pump is smaller than in the magnetic field approach. Thus, it allows us to reconcile why the observed photoinduced effect corresponds to the relatively weak H -field.

Discussion

Using the tr-RSXS study on the CDW behavior in YBCO, we explore the intertwined phenomena between the CDW and SC in the normal state induced by the optical pump. We reveal that the CDW characteristic behaviors in the non-equilibrium state show close similarity with those under the magnetic field. Clearly, these findings could provide a clue that the transient state characteristics show a solid analogy to the normal state under equilibrium conditions demonstrated by the magnetic field.

Beyond this, we further discuss the implications of our finding. The fact that CDW and/or spin density wave (SDW) orders in high- T_c cuprates are enhanced by the external magnetic field (24,26-28,47–49) indicates that the vortex state is related to the quenched SC by H -field. Such a circumstance is depicted as cartoons in Figs. 5A and 5B (top panel). As the external magnetic field is increased, the number of vortices corresponding increases, leading to an increase in the fraction of the quenched SC volume (i.e., increase in the normal state fraction) in the CuO_2 plane (49). In the same manner, we depict that the Cooper-paired SC states (Fig. 5A) are transformed into the broken/weakened Cooper pairs through a proper optical pump (Fig. 5B, bottom panel) (33–40). For a short while, it leads to a transient state that becomes dominant over the reduced

SC portion in the CuO_2 plane. After all, the two approaches through the optical pump and the external magnetic field drive the quenched SC state, and their corresponding CDW responses are characteristically identical to the normal state. In this sense, we infer that an essential physics in the non-equilibrium state would be in a crossover with the equilibrium physics. This inference suggests that expanding the vortex liquid state by increasing the magnetic field could be alternatively interpreted by physics of the broken Cooper-pairing in the CuO_2 plane (see Fig. 5C). Ultimately, it implies that demonstrating the quenched SC state with either approach could be delivering the equivalent physics in HTSC. Inversely, with the equilibrium state, it is considerable that optical pump approaches are possible to drive room temperature transient superconductivity (41–44). Moreover, understanding such a discussion presents a rich opportunity for detailed experimental investigations (e.g., CDW study through synchronizing three pulses between x-ray, an optical pump, and magnetic field) and theoretical interpretations in the future.

Materials and Methods

Sample preparation. Single crystals of $\text{YBa}_2\text{Cu}_3\text{O}_{6.67}$ ($T_c = 65.5$ K) were grown using a flux method (50), and the oxygen content was adjusted by annealing under well-defined oxygen partial pressure. The sample was mechanically detwinned by heating under uniaxial stress (50 ~ 60 MPa was applied at 400 °C). The dimensions of the single crystal were 2.10 mm \times 1.05 mm \times 0.38 mm along the crystallographic a , b , and c -axis, respectively (lattice parameters: $a \sim 3.82$ Å, $b \sim 3.88$ Å, and $c \sim 11.725$ Å). The single crystal was thoroughly characterized by measuring the static CDW signal at the Stanford Synchrotron Radiation Lightsource (SSRL) beamline 13-3, using Cu L_3 -edge resonant soft x-ray scattering (RSXS) measurements (fig. S1).

tr-RSXS measurement. All tr-RSXS experiments were carried out at the SSS-RSXS endstation of PAL-XFEL (51). The sample was mounted on a 6-axis open-circle cryostat manipulator and a base temperature of ~15 K using liquid helium. The sample surface was perpendicular to the crystalline c -axis, and the horizontal scattering plan was parallel to the bc -plane. X-ray pulses with an ~80 fs pulse duration and a 60 Hz repetition rate were used for the soft x-ray probe. The x-ray was linearly and horizontally polarized (π -polarization) and the photon energy was tuned around the Cu L_3 -edge (932 eV). A 1.55 eV (800 nm) optical laser pump with a ~50 fs pulse

duration and p -polarization was provided by a Ti:sapphire laser (see Fig. 2A and fig. S7). It is commonly appreciated that the laser pulses at 800 nm are able to strongly perturb superconductivity in cuprates (33–35, 39, 40, 52–55). The optical laser was nearly parallel to the incident x-ray beam as the angle difference is less than 1° . A pump fluence of $15 \mu\text{J}/\text{cm}^2$ was mainly used (see fig. S5). The time delay between pump and probe pulses was controlled by a mechanical delay stage. The spot size of the x-ray at the sample position was $100 \text{ (H)} \times 200 \text{ (V)} \mu\text{m}^2$ in FWHM and the spot diameter of optical laser was $\sim 500 \mu\text{m}$ in FWHM. The x-ray scattering signal was collected by an avalanche photodiode (APD), which was enclosed in an aluminum cage, and the front was covered by a 300-nm-thick aluminum filter to ensure light tightness. All signals were recorded by high-speed digitizers and analyzed on a shot-to-shot basis.

X-ray scattering measurement with a high magnetic field. The high field pulsed-magnet experiments were performed at the BL2-EH3 hutch of the SACLA (56). The YBCO sample was attached on a sapphire rod. The rod was mounted on a closed-cycle cryocooler with a capability of a sample base temperature $\sim 10 \text{ K}$. X-ray pulses with a 7 fs pulse duration and a 30 Hz repetition rate were used. The x-ray was linearly and horizontally polarized (π -polarization) and the photon energy was tuned to 8.8 keV, just below the Cu K -edge to reduce the fluorescence background (26). X-ray pulse arrived at the top of $\sim 1 \text{ ms}$ duration pulsed magnetic field with $\sim 30 \text{ Tesla}$. To obtain zero-field background, 10 shots of x-ray only scattering signal were obtained before and after the shot with a magnetic pulse. As shown in Fig. 4c, therefore, the noise levels between $H = 0 \text{ T}$ (80 shots accumulated) and 30 T (4 shots) appear differently (see fig. S9). A half-mega pixel Multi-Port Charge-Coupled Device (MPCCD) was used to capture the 2D scattering profile.

References

1. J. G. Bednorz, K. A. Müller, Possible high T_c superconductivity in the Ba–La–Cu–O system. *Z. Physik B* **64**, 189–193 (1986). <https://doi.org/10.1007/BF01303701>
2. E. Fradkin, S. A. Kivelson, Ineluctable complexity. *Nat. Phys.* **8**, 864–866 (2012). <https://doi.org/10.1038/nphys2498>
3. E. Fradkin, S. A. Kivelson, J. M. Tranquada, Colloquium: Theory of intertwined orders in high temperature superconductors. *Rev. Mod. Phys.* **87**, 457–482 (2015). <https://doi.org/10.1103/RevModPhys.87.457>
4. B. Keimer, S. A. Kivelson, M. R. Norman, S. Uchida, J. Zaanen., From quantum matter to high-temperature superconductivity in copper oxides. *Nature* **518**, 179–186 (2015). <https://doi.org/10.1038/nature14165>
5. C. M. Varma, P. B. Littlewood, S. Schmitt-Rink, E. Abrahams, A. E. Ruckenstein, Phenomenology of the normal state of Cu-O high-temperature superconductors. *Phys. Rev. Lett.* **63**, 1996–1999 (1989). <https://doi.org/10.1103/PhysRevLett.63.1996>
6. T. Timusk, B. Statt, The pseudogap in high-temperature superconductors: an experimental survey. *Rep. Prog. Phys.* **62**, 61–122 (1999). <https://doi.org/10.1103/10.1088/0034-4885/62/1/002>
7. J. M. Tranquada, B. J. Sternlieb, J. D. Axe, Y. Nakamura, S. Uchida, Evidence for stripe correlations of spins and holes in copper oxide superconductors. *Nature* **375**, 561–563 (1995). <https://doi.org/10.1038/375561a0>
8. S. A. Kivelson, E. Fradkin, V. J. Emery, Electronic liquid-crystal phases of a doped Mott insulator. *Nature* **393**, 550–553 (1998). <http://doi.org/10.1038/31177>
9. S. A. Kivelson, I. P. Bindloss, E. Fradkin, V. Oganessian, J. M. Tranquada, A. Kapitulnik, C. Howald, How to detect fluctuating stripes in the high-temperature superconductors. *Rev. Mod. Phys.* **75**, 1201–1241 (2003). <http://doi.org/10.1103/RevModPhys.75.1201>
10. J. E. Hoffman, E. W. Hudson, K. M. Lang, V. Madhavan, H. Eisaki, S. Uchida, J. C. Davis, A Four Unit Cell Periodic Pattern of Quasi-Particle States Surrounding Vortex Cores in $\text{Bi}_2\text{Sr}_2\text{CaCu}_2\text{O}_{8+\delta}$. *Science* **295**, 466–469 (2002). <http://doi.org/10.1126/science.1066974>
11. P. Abbamonte, A. Rusydi, S. Smadici, G. D. Gu, G. A. Sawatzky, D. L. Feng, Spatially modulated ‘Mottness’ in $\text{La}_{2-x}\text{Ba}_x\text{CuO}_4$. *Nat. Phys.* **1**, 155–158 (2005). <http://doi.org/10.1038/nphys178>

12. G. Ghiringhelli, M. L. Tacon, M. Minola, S. Blanco-Canosa, C. Mazzoli, N. B. Brookes, G. M. D. Luca, A. Frano, D. G. Hawthorn, F. He, T. Loew, M. M. Sala, D. C. Peets, M. Salluzzo, E. Schierle, R. Sutarto, G. A. Sawatzky, E. Weschke, B. Keimer, L. Braicovich, Long-Range Incommensurate Charge Fluctuations in (Y,Nd)Ba₂Cu₃O_{6+x}. *Science* **337**, 821–825 (2012). <http://doi.org/10.1126/science.1223532>
13. S. Blanco-Canosa, A. Frano, E. Schierle, J. Porras, T. Loew, M. Minola, M. Bluschke, E. Weschke, B. Keimer, M. Le Tacon, Resonant x-ray scattering study of charge-density wave correlations in YBa₂Cu₃O_{6+x}. *Phys. Rev. B* **90**, 054513 (2014). <http://doi.org/10.1103/PhysRevB.90.054513>
14. T. Wu, H. Mayaffre, S. Krämer, M. Horvatić, C. Berthier, W.N. Hardy, R. Liang, D.A. Bonn, M.-H. Julien, Magnetic-field-induced charge-stripe order in the high-temperature superconductor YBa₂Cu₃O_y. *Nature* **477**, 191–194 (2011). <http://doi.org/10.1038/nature10345>
15. R. Comin, A. Frano, M.M. Yee, Y. Yoshida, H. Eisaki, E. Schierle, E. Weschke, R. Sutarto, F. He, A. Soumyanarayanan, Y. He, M. L. Tacon, I. S. Elfimov, J.E. Hoffman, G. A. Sawatzky, B. Keimer, A. Damascelli, Charge Order Driven by Fermi-Arc Instability in Bi₂Sr_{2-x}La_xCuO_{6+δ}. *Science* **343**, 390–392 (2014). <http://doi.org/10.1126/science.1242996>
16. W. Tabis, Y. Li, M.L. Tacon, L. Braicovich, A. Kreyssig, M. Minola, G. Dellea, E. Weschke, M. J. Veit, M. Ramazanoglu, A. I. Goldman, T. Schmitt, G. Ghiringhelli, N. Barišić, M. K. Chan, C. J. Dorow, G. Yu, X. Zhao, B. Keimer, M. Greven, Charge order and its connection with Fermi-liquid charge transport in a pristine high-*T_c* cuprate. *Nat. Commun.* **5**, 5875 (2014). <http://doi.org/10.1038/ncomms6875>
17. E. H. da Silva Neto, R. Comin, F. He, R. Sutarto, Y. Jiang, R. L. Greene, G. A. Sawatzky, Charge ordering in the electron-doped superconductor Nd_{2-x}Ce_xCuO₄. *Science* **347**, 282–285 (2015). <http://doi.org/10.1126/science.1256441>
18. H. Jang, S. Asano, M. Fujita, M. Hashimoto, D. H. Lu, C. A. Burns, C.-C. Kao, J.-S. Lee, Superconductivity-Insensitive Order at $q \sim 1/4$ in Electron-Doped Cuprates. *Phys. Rev. X* **7**, 041066 (2017). <http://doi.org/10.1103/PhysRevX.7.041066>
19. H. Miao, J. Lorenzana, G. Seibold, Y. Y. Peng, A. Amorese, F. Yakhou-Harris, K. Kummer, N. B. Brookes, R. M. Konik, V. Thampy, G. D. Gu, G. Ghiringhelli, L. Braicovich, M. P. M. Dean, High-temperature charge density wave correlations in La_{1.875}Ba_{0.125}CuO₄ without spin-

- charge locking. *Proc. Natl Acad. Sci. USA* **114**, 12430–12435 (2017).
<http://doi.org/10.1073/pnas.1708549114>
20. J.-J. Wen, H. Huang, S.-J. Lee, H. Jang, J. Knight, Y. S. Lee, M. Fujita, K. M. Suzuki, S. Asano, S. A. Kivelson, C.-C. Kao, J.-S. Lee, Observation of two types of charge-density-wave orders in superconducting $\text{La}_{2-x}\text{Sr}_x\text{CuO}_4$. *Nat. Commun.* **10**, 3269 (2019).
<http://doi.org/10.1038/s41467-019-11167-z>
21. N. Miura, H. Nakagawa, T. Sekitani, M. Naito, H. Sato, Y. Enomoto, High-magnetic-field study of high- T_c cuprates. *Physica B* **319**, 310–320 (2002). [http://doi.org/10.1016/S0921-4526\(02\)01134-1](http://doi.org/10.1016/S0921-4526(02)01134-1)
22. G. Grissonnanche, O. Cyr-Choinière, F. Laliberté, S. René de Cotret, A. Juneau-Fecteau, S. Dufour-Beauséjour, M.-È. Delage, D. LeBoeuf, J. Chang, B. J. Ramshaw, D. A. Bonn, W. N. Hardy, R. Liang, S. Adachi, N. E. Hussey, B. Vignolle, C. Proust, M. Sutherland, S. Krämer, J.-H. Park, D. Graf, N. Doiron-Leyraud, L. Taillefer, Direct measurement of the upper critical field in cuprate superconductors. *Nat. Commun.* **5**, 3280 (2014).
<http://doi.org/10.1038/ncomms4280>
23. J. B. Kemper, O. Vafek, J. B. Betts, F. F. Balakirev, W. N. Hardy, R. Liang, D. A. Bonn, G. S. Boebinger, Thermodynamic signature of a magnetic-field-driven phase transition within the superconducting state of an underdoped cuprate. *Nat. Phys.* **12**, 47–51 (2016).
<http://doi.org/10.1038/nphys3502>
24. J. Chang, E. Blackburn, A. T. Holmes, N. B. Christensen, J. Larsen, J. Mesot, R. Liang, D. A. Bonn, W. N. Hardy, A. Watenphul, M. v Zimmermann, E. M. Forgan, S. M. Hayden, Direct observation of competition between superconductivity and charge density wave order in $\text{YBa}_2\text{Cu}_3\text{O}_{6.67}$. *Nat. Phys.* **8**, 871–876 (2012). <http://doi.org/10.1038/nphys2456>
25. S. Blanco-Canosa, A. Frano, T. Loew, Y. Lu, J. Porras, G. Ghiringhelli, M. Minola, C. Mazzoli, L. Braicovich, E. Schierle, E. Weschke, M. Le Tacon, B. Keimer, Momentum-Dependent Charge Correlations in $\text{YBa}_2\text{Cu}_3\text{O}_{6+\delta}$ Superconductors Probed by Resonant X-Ray Scattering: Evidence for Three Competing Phases. *Phys. Rev. Lett.* **110**, 187001 (2013).
<http://doi.org/10.1103/PhysRevLett.110.187001>
26. S. Gerber, H. Jang, H. Nojiri, S. Matsuzawa, H. Yasumura, D. A. Bonn, R. Liang, W. N. Hardy, Z. Islam, A. Mehta, S. Song, M. Sikorski, D. Stefanescu, Y. Feng, S. A. Kivelson, T. P. Devereaux, Z.-X. Shen, C.-C. Kao, W.-S. Lee, D. Zhu, J.-S. Lee, Three-dimensional

- charge density wave order in $\text{YBa}_2\text{Cu}_3\text{O}_{6.67}$ at high magnetic fields. *Science* **350**, 949–952 (2015). <http://doi.org/10.1126/science.aac6257>
27. J. Chang, E. Blackburn, O. Ivashko, A. T. Holmes, N. B. Christensen, M. Hücker, R. Liang, D. A. Bonn, W. N. Hardy, U. Rütt, M. v Zimmermann, E. M. Forgan, S. M. Hayden, Magnetic field controlled charge density wave coupling in underdoped $\text{YBa}_2\text{Cu}_3\text{O}_{6+x}$. *Nat. Commun.* **7**, 11494 (2016). <http://doi.org/10.1038/ncomms11494>
 28. H. Jang, W.-S. Lee, H. Nojiri, S. Matsuzawa, H. Yasumura, L. Nie, A. V. Maharaj, S. Gerber, Y.-J. Liu, A. Mehta, D. A. Bonn, R. Liang, W. N. Hardy, C. A. Burns, Z. Islam, S. Song, J. Hastings, T. P. Devereaux, Z.-X. Shen, S. A. Kivelson, C.-C. Kao, D. Zhu, J.-S. Lee, Ideal charge-density-wave order in the high-field state of superconducting YBCO. *Proc. Natl Acad. Sci. USA* **113**, 14645–14650 (2016). <http://doi.org/10.1073/pnas.1612849113>
 29. H. Jang, W.-S. Lee, S. Song, H. Nojiri, S. Matsuzawa, H. Yasumura, H. Huang, Y.-J. Liu, J. Porras, M. Minola, B. Keimer, J. Hastings, D. Zhu, T. P. Devereaux, Z.-X. Shen, C.-C. Kao, J.-S. Lee, Coincident onset of charge-density-wave order at a quantum critical point in underdoped $\text{YBa}_2\text{Cu}_3\text{O}_x$. *Phys. Rev. B* **97**, 224513 (2018). <http://doi.org/10.1103/PhysRevB.97.224513>
 30. J. Choi, O. Ivashko, E. Blackburn, R. Liang, D. A. Bonn, W. N. Hardy, A. T. Holmes, N. B. Christensen, M. Hücker, S. Gerber, O. Gutowski, U. Rütt, M. v Zimmermann, E. M. Forgan, S. M. Hayden, J. Chang, Spatially inhomogeneous competition between superconductivity and the charge density wave in $\text{YBa}_2\text{Cu}_3\text{O}_{6.67}$. *Nat. Commun.* **11**, 990 (2020). <http://doi.org/10.1038/s41467-020-14536-1>
 31. C. Giannetti, M. Capone, D. Fausti, M. Fabrizio, F. Parmigiani, D. Mihailovic, Ultrafast optical spectroscopy of strongly correlated materials and high-temperature superconductors: a non-equilibrium approach. *Adv. Phys.* **65**, 58–238 (2016). <http://doi.org/10.1080/00018732.2016.1194044>
 32. J. Demsar, Non-equilibrium Phenomena in Superconductors Probed by Femtosecond Time-Domain Spectroscopy. *J. Low Temp. Phys.* **201**, 676–709 (2020). <http://doi.org/10.1007/s10909-020-02461-y>
 33. R. A. Kaindl, M. Woerner, T. Elsaesser, D. C. Smith, J. F. Ryan, G. A. Farnan, M. P. McCurry, D. G. Walmsley, Ultrafast Mid-Infrared Response of $\text{YBa}_2\text{Cu}_3\text{O}_{7-\delta}$. *Science* **287**, 470–473 (2000). <http://doi.org/10.1126/science.287.5452.470>

34. P. Kusar, V. V. Kabanov, J. Demsar, T. Mertelj, S. Sugai, D. Mihailovic, Controlled Vaporization of the Superconducting Condensate in Cuprate Superconductors by Femtosecond Photoexcitation. *Phys. Rev. Lett.* **101**, 227001 (2008).
<http://doi.org/10.1103/PhysRevLett.101.227001>
35. L. Stojchevska, P. Kusar, T. Mertelj, V. V. Kabanov, Y. Toda, X. Yao, D. Mihailovic, Mechanisms of nonthermal destruction of the superconducting state and melting of the charge-density-wave state by femtosecond laser pulses. *Phys. Rev. B* **84**, 180507 (2011).
<http://doi.org/10.1103/PhysRevB.84.180507>
36. J. P. Hinton, J. D. Koralek, Y. M. Lu, A. Vishwanath, J. Orenstein, D. A. Bonn, W. N. Hardy, R. Liang, New collective mode in $\text{YBa}_2\text{Cu}_3\text{O}_{6+x}$ observed by time-domain reflectometry. *Phys. Rev. B* **88**, 060508 (2013). <http://doi.org/10.1103/PhysRevB.88.060508>
37. G. Coslovich, C. Giannetti, F. Cilento, S. Dal Conte, G. Ferrini, P. Galinetto, M. Greven, H. Eisaki, M. Raichle, R. Liang, A. Damascelli, F. Parmigiani, Evidence for a photoinduced nonthermal superconducting-to-normal-state phase transition in overdoped $\text{Bi}_2\text{Sr}_2\text{Ca}_{0.92}\text{Y}_{0.08}\text{Cu}_2\text{O}_{8+\delta}$. *Phys. Rev. B* **83**, 064519 (2011).
<http://doi.org/10.1103/PhysRevB.83.064519>
38. G. Coslovich, C. Giannetti, F. Cilento, S. Dal Conte, T. Abebaw, D. Bossini, G. Ferrini, H. Eisaki, M. Greven, A. Damascelli, F. Parmigiani, Competition Between the Pseudogap and Superconducting States of $\text{Bi}_2\text{Sr}_2\text{Ca}_{0.92}\text{Y}_{0.08}\text{Cu}_2\text{O}_{8+\delta}$ Single Crystals Revealed by Ultrafast Broadband Optical Reflectivity. *Phys. Rev. Lett.* **110**, 107003 (2013).
<http://doi.org/10.1103/PhysRevLett.110.107003>
39. F. Boschini, E. H. da Silva Neto, E. Razzoli, M. Zonno, S. Peli, R. P. Day, M. Michiardi, M. Schneider, B. Zwartsenberg, P. Nigge, R. D. Zhong, J. Schneeloch, G. D. Gu, S. Zhdanovich, A. K. Mills, G. Levy, D. J. Jones, C. Giannetti, A. Damascelli, Collapse of superconductivity in cuprates via ultrafast quenching of phase coherence. *Nat. Mater.* **17**, 416–420 (2018).
<http://doi.org/10.1038/s41563-018-0045-1>
40. S. Wandel, F. Boschini, E. H. da S. Neto, L. Shen, M. X. Na, S. Zohar, Y. Wang, G. B. Welch, M. H. Seaberg, J. D. Koralek, G. L. Dakovski, W. Hettel, M.-F. Lin, S. P. Moeller, W. F. Schlotter, A. H. Reid, M. P. Minitti, T. Boyle, F. He, R. Sutarto, R. Liang, D. Bonn, W. Hardy, R. A. Kaindl, D. G. Hawthorn, J.-S. Lee, A. F. Kemper, A. Damascelli, C.

- Giannetti, J. J. Turner, G. Coslovich, Light-enhanced Charge Density Wave Coherence in a High-Temperature Superconductor. Preprint at <https://arxiv.org/abs/2003.04224> (2020)
41. W. Hu, S. Kaiser, D. Nicoletti, C. R. Hunt, I. Gierz, M. C. Hoffmann, M. Le Tacon, T. Loew, B. Keimer, A. Cavalleri, Optically enhanced coherent transport in $\text{YBa}_2\text{Cu}_3\text{O}_{6.5}$ by ultrafast redistribution of interlayer coupling. *Nat. Mater.* **13**, 705–711 (2014).
<http://doi.org/10.1038/nmat3963>
42. S. Kaiser, C. R. Hunt, D. Nicoletti, W. Hu, I. Gierz, H. Y. Liu, M. Le Tacon, T. Loew, D. Haug, B. Keimer, A. Cavalleri, Optically induced coherent transport far above T_c in underdoped $\text{YBa}_2\text{Cu}_3\text{O}_{6+\delta}$. *Phys. Rev. B* **89**, 184516 (2014).
<https://doi.org/10.1103/PhysRevB.89.184516>
43. R. Mankowsky, A. Subedi, M. Först, S. O. Mariager, M. Chollet, H. T. Lemke, J. S. Robinson, J. M. Glownia, M. P. Minitti, A. Frano, M. Fechner, N. A. Spaldin, T. Loew, B. Keimer, A. Georges, A. Cavalleri, Nonlinear lattice dynamics as a basis for enhanced superconductivity in $\text{YBa}_2\text{Cu}_3\text{O}_{6.5}$. *Nature* **516**, 71–73 (2014).
<https://doi.org/10.1038/nature13875>
44. B. Liu, M. Först, M. Fechner, D. Nicoletti, J. Porras, T. Loew, B. Keimer, A. Cavalleri, Pump Frequency Resonances for Light-Induced Incipient Superconductivity in $\text{YBa}_2\text{Cu}_3\text{O}_{6.5}$. *Phys. Rev. X* **10**, 011053 (2020). <http://doi.org/10.1103/PhysRevX.10.011053>
45. B. J. Ramshaw, J. Day, B. Vignolle, D. LeBoeuf, P. Dosanjh, C. Proust, L. Taillefer, R. Liang, W. N. Hardy, D. A. Bonn, Vortex lattice melting and H_{c2} in underdoped $\text{YBa}_2\text{Cu}_3\text{O}_y$. *Phys. Rev. B* **86**, 174501 (2012). <http://doi.org/10.1103/PhysRevB.86.174501>
46. C. Marcenat, A. Demuer, K. Beauvois, B. Michon, A. Grockowiak, R. Liang, W. Hardy, D. A. Bonn, T. Klein, Calorimetric determination of the magnetic phase diagram of underdoped ortho II $\text{YBa}_2\text{Cu}_3\text{O}_{6.54}$ single crystals. *Nat. Commun.* **6**, 7927 (2015).
<http://doi.org/10.1038/ncomms8927>
47. B. Lake, K. Lefmann, N. B. Christensen, G. Aeppli, D. F. McMorrow, H. M. Ronnow, P. Vorderwisch, P. Smeibidl, N. Mangkorntong, T. Sasagawa, M. Nohara, H. Takagi, Three-dimensionality of field-induced magnetism in a high-temperature superconductor. *Nat. Mater.* **4**, 658–662 (2005). <http://doi.org/10.1038/nmat1452>
48. Y. Yu, S. A. Kivelson, Fragile superconductivity in the presence of weakly disordered charge density waves. *Phys. Rev. B* **99**, 144513 (2019). <http://doi.org/10.1103/PhysRevB.99.144513>

49. Z. Shi, P. G. Baity, T. Sasagawa, D. Popović, Vortex phase diagram and the normal state of cuprates with charge and spin orders. *Sci. Adv.* **6**, eaay8946 (2020).
<http://doi.org/10.1126/sciadv.aay8946>
50. V. Hinkov, S. Pailhès, P. Bourges, Y. Sidis, A. Ivanov, A. Kulakov, C. T. Lin, D. P. Chen, C. Bernhard, B. Keimer, Two-dimensional geometry of spin excitations in the high-transition-temperature superconductor $\text{YBa}_2\text{Cu}_3\text{O}_{6+x}$. *Nature* **430**, 650 (2004).
<https://doi.org/10.1038/nature02774>
51. H. Jang, H.-D. Kim, M. Kim, S. H. Park, S. Kwon, J.Y. Lee, S.-Y. Park, G. Park, S. Kim, H. Hyun, S. Hwang, C.-S. Lee, C.-Y. Lim, W. Gang, M. Kim, S. Heo, J. Kim, G. Jung, S. Kim, J. Park, J. Kim, H. Shin, J. Park, T.-Y. Koo, H.-J. Shin, H. Heo, C. Kim, C.-K. Min, J.-H. Han, H.-S. Kang, H.-S. Lee, K.S. Kim, I. Eom, S. Rah, Time-resolved resonant elastic soft x-ray scattering at Pohang Accelerator Laboratory X-ray Free Electron Laser. *Rev. Sci. Instrum.* **91**, 083904 (2020). <https://doi.org/10.1063/5.0016414>
52. L. Perfetti, P. A. Loukakos, M. Lisowski, U. Bovensiepen, H. Eisaki, M. Wolf, Ultrafast Electron Relaxation in Superconducting $\text{Bi}_2\text{Sr}_2\text{CaCu}_2\text{O}_{8+\delta}$ by Time-Resolved Photoelectron Spectroscopy, *Phys. Rev. Lett.* **99**, 197001 (2007).
<https://doi.org/10.1103/PhysRevLett.99.197001>
53. J. Demsar, B. Podobnik, V. V. Kabanov, Th. Wolf, D. Mihailovic, Superconducting Gap Δ_c , the Pseudogap Δ_p , and Pair Fluctuations above T_c in Overdoped $\text{Y}_{1-x}\text{Ca}_x\text{Ba}_2\text{Cu}_3\text{O}_{7-\delta}$ from Femtosecond Time-Domain Spectroscopy. *Phys. Rev. Lett.* **82**, 4918 (1999).
<https://doi.org/10.1103/PhysRevLett.82.4918>
54. R. D. Averitt, G. Rodriguez, A. I. Lobad, J. L. W. Siders, S. A. Trugman, and A. J. Taylor, Nonequilibrium superconductivity and quasiparticle dynamics in $\text{YBa}_2\text{Cu}_3\text{O}_{7-\delta}$. *Phys. Rev. B* **63**, 140502(R) (2001). <https://doi.org/10.1103/PhysRevB.63.140502>
55. M. Mitrano, S. Lee, A. A. Husain, L. Delacretaz, M. Zhu, G. de la Peña Muñoz, S. X.-L. Sun, Y. I. Joe, A. H. Reid, S. F. Wandel, G. Coslovich, W. Schlotter, T. van Driel, J. Schneeloch, G. D. Gu, S. Hartnoll, N. Goldenfeld, P. Abbamonte, Ultrafast time-resolved x-ray scattering reveals diffusive charge order dynamics in $\text{La}_{2-x}\text{Ba}_x\text{CuO}_4$. *Sci. Adv.* **5**, eaax3346 (2019). <https://doi.org/10.1126/sciadv.aax3346>
56. T. Ishikawa, H. Aoyagi, T. Asaka, Y. Asano, N. Azumi, T. Bizen, H. Ego, K. Fukami, T. Fukui, Y. Furukawa, S. Goto, H. Hanaki, T. Hara, T. Hasegawa, T. Hatsui, A. Higashiya, T.

Hirono, N. Hosoda, M. Ishii, T. Inagaki, Y. Inubushi, T. Itoga, Y. Joti, M. Kago, T. Kameshima, H. Kimura, Y. Kirihara, A. Kiyomichi, T. Kobayashi, C. Kondo, T. Kudo, H. Maesaka, X.M. Maréchal, T. Masuda, S. Matsubara, T. Matsumoto, T. Matsushita, S. Matsui, M. Nagasono, N. Nariyama, H. Ohashi, T. Ohata, T. Ohshima, S. Ono, Y. Otake, C. Saji, T. Sakurai, T. Sato, K. Sawada, T. Seike, K. Shirasawa, T. Sugimoto, S. Suzuki, S. Takahashi, H. Takebe, K. Takeshita, K. Tamasaku, H. Tanaka, R. Tanaka, T. Tanaka, T. Togashi, K. Togawa, A. Tokuhisa, H. Tomizawa, K. Tono, S. Wu, M. Yabashi, M. Yamaga, A. Yamashita, K. Yanagida, C. Zhang, T. Shintake, H. Kitamura, N. Kumagai, A compact X-ray free-electron laser emitting in the sub-ångström region. *Nat. Photon.* **6**, 540–544 (2012).
<https://doi.org/10.1038/nphoton.2012.141>

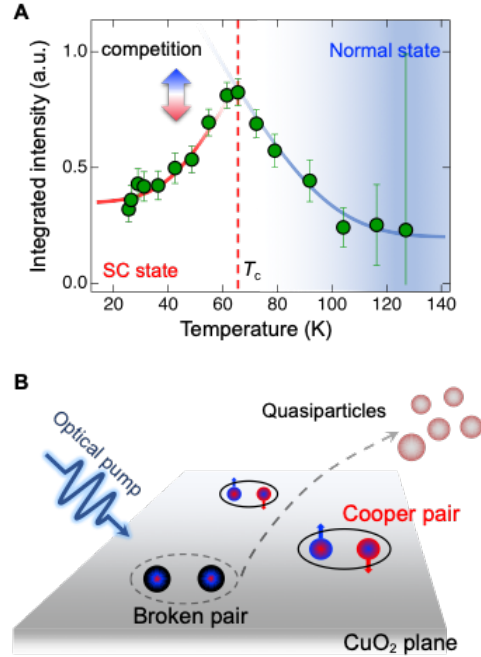


Fig. 1. Normal and superconducting states in the CuO_2 plane of the YBCO. (A) Temperature dependence of a static CDW order. It shows the integrated intensity of CDW peak at $Q = (0, q_{\text{cdw}}, \sim 1.45)$ as a function of temperature, where q_{cdw} is around -0.32 r.l.u. The CDW emerges below ~ 150 K. Below $T_c = 65.5$ K (dashed line), the CDW peak becomes suppressed with the development of the SC. Solid lines are guides-to-the-eye. (B) A schematic sketch for the optical pump effect in a superconducting CuO_2 plane. The solid and dashed ellipses are a superconducting Cooper pair state and its broken state, respectively. The broken pairs transform to quasiparticles due to an optical pump.

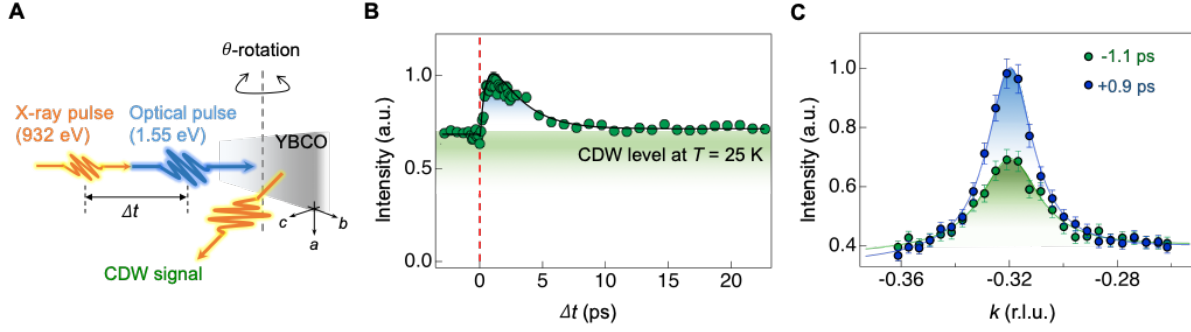


Fig. 2. Time-resolved resonant soft x-ray scattering (tr-RSXS) on YBCO. (A) Schematic experimental configuration for YBCO sample. The orange and blue colored pulses denote x-ray (932 eV, Cu L_3 -edge) and optical laser (1.55 eV), respectively. θ -scans were performed to find a CDW peak at $Q = (0, q_{\text{cdw}}, 1)$. (B) CDW intensity at $Q = (0, q_{\text{cdw}}, \sim 1.45)$ as a function of Δt , measured at $T = 25$ K (below T_c). For $\Delta t < 0$, the CDW height indicates the suppressed, but non-zero, CDW due to the competition with SC. For $0 < \Delta t < \sim 7$ ps, the CDW height is enhanced by the optical pump. The solid line presents a fit to exponential functions. The dashed line indicates $\Delta t = 0$. (C) The CDW peak profiles at $\Delta t = -1.1$ ps (i.e., before pumping) and $\Delta t = +0.9$ ps (i.e., maximum pumping effect on CDW). Solid lines are Lorentzian fits to the data with a linear background. Green and blue colored shades are guides-to-the-eye to denote unpumped (i.e., static) and photoinduced CDW, respectively.

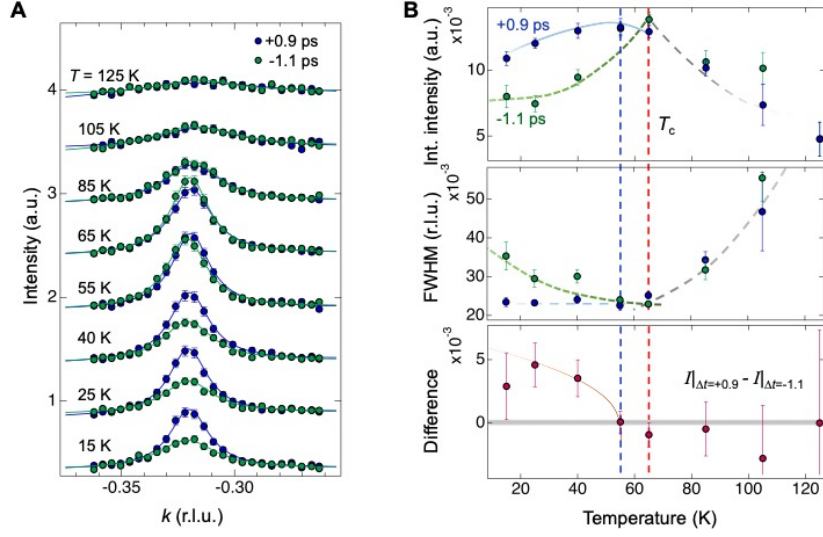


Fig. 3. Temperature dependence of photoinduced CDW. (A) The CDW peak profiles at $(0, k, \sim 1.45)$ measured at $\Delta t = +0.9$ ps (blue) and -1.1 ps (green) with varying sample temperature. Solid lines are Lorentzian fits to the data with a linear background. (B) Fitted results of temperature dependence at $\Delta t = +0.9$ ps (blue) and -1.1 ps (green) for (top panel) integrated intensity and (middle panel) peak width (full-width at half maximum, FWHM). Bottom panel shows a difference of integrated intensities between $\Delta t = +0.9$ ps and -1.1 ps. Red and blue vertical dashed lines respectively represent T_c before ($\Delta t < 0$) and after ($\Delta t = +0.9$ ps) optical pumping. Solid and dashed lines are guides-to-eye. The error bars represent 1 standard deviation (s.d.) of the fit parameters.

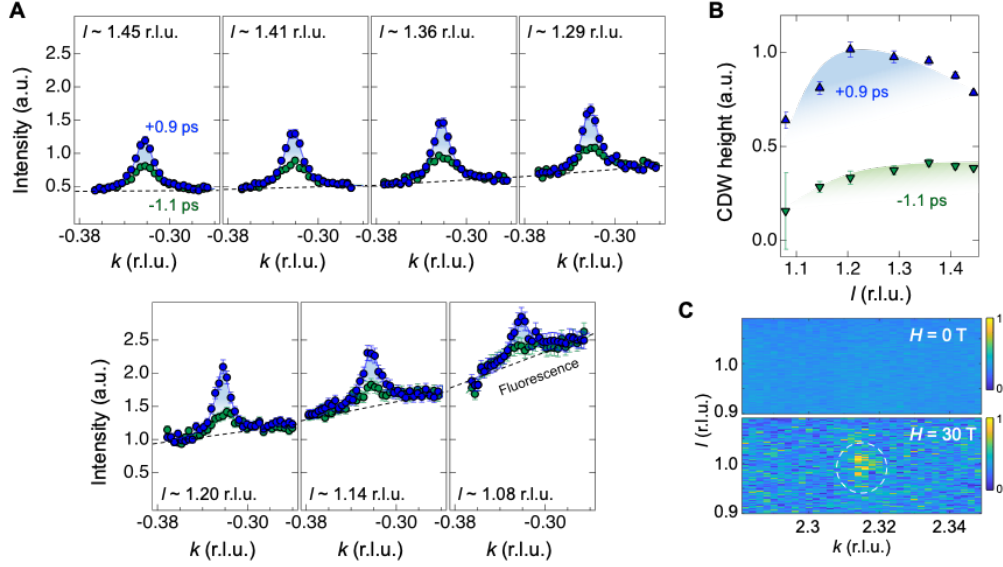


Fig. 4. L -dependence of photoinduced CDW. (A) The CDW peak profiles of YBCO measured at $\Delta t = +0.9$ ps and -1.1 ps with varying detector positions (i.e., L -dependence) and $T = 25$ K. The dashed lines indicate a fluorescence background slope at each geometrical (detector) position. As detector 2θ decreases (i.e., l decreases), the fluorescence background is more pronounced due to geometrical effects such as elongation of the beam footprint. Solid lines are Lorentzian fits to the data with a linear fluorescence background. (B) Fitted CDW heights with the different l -position (i.e., 2θ) at $\Delta t = +0.9$ ps (up-triangles) and -1.1 ps (down-triangles). Blue and green colored shades are guides-to-the-eye. The error bars represent 1 s.d. of the fit parameters. (C) The observed 3D CDW of YBCO via a pulsed magnet experiment (see Method). The field-induced CDW appears (4 shots average) around $(0, 2+q_{\text{cdw}}, 1)$, compared to the zero field (80 shots average).

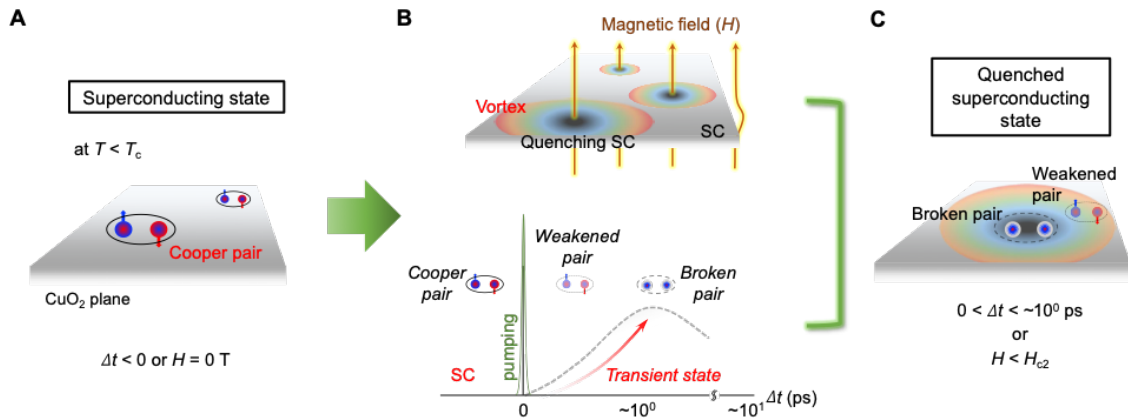


Fig. 5. Connection between equilibrium and non-equilibrium states. (A) Schematic cartoon of YBCO's superconducting state below T_c . The presence of Cooper pairs denotes SC. (B) Two independent ways to quench SC of YBCO, transforming into the normal state. Top and bottom panels are an external magnetic field approach (representing the equilibrium state) and optical pumping approach (representing the non-equilibrium state), respectively. The magnetic field approach causes the nucleation of the vortex state; the optical pumping denotes three kinds of pairing states (schematic inset: initial Cooper pair, weakened pair, and broken pair) within negative to a picosecond time frame, while SC state is transformed to a transient normal state. (C) A characterization of transient state in YBCO. The quenched SC states by either the vortex or the increased distribution of the broken (or weakened) pairs, are equivalent.

Supplementary Materials for

Characterization of photoinduced normal state through charge density wave in superconducting $\text{YBa}_2\text{Cu}_3\text{O}_{6.67}$

H. Jang, S. Song, T. Kihara, Y. Liu, S.-J. Lee, S.-Y. Park, M. Kim, H.-D. Kim, G. Coslovich, S. Nakata, Y. Kubota, I. Inoue, K. Tamasaku, M. Yabashi, H. Lee, C. Song, H. Nojiri, B. Keimer, C.-C. Kao, and J.-S. Lee*

*Corresponding author. Email: jslee@slac.stanford.edu

- **RSXS measurement:** The RSXS measurements were carried out at beamline 13-3 of the Stanford Synchrotron Radiation Lightsource (SSRL). The sample was mounted on an in-vacuum 4-circle diffractometer. The sample temperature was controlled by an open-circle helium cryostat. The x-ray was linearly and vertically polarized (σ -polarization), and the photon energy was tuned around Cu L_3 -edge (932 eV). The exact $(0, k, l)$ scattering plane was aligned by the measured $(0, 0, 2)$, $(0, -1, 1)$, and $(1, 0, 1)$ structural Bragg reflections at the photon energy ~ 1770 eV. The scattering signal was obtained by a GaAs photodiode and normalized by the drain current on Au mesh.

- **Analysis of transient behavior of the CDW intensity:** To analyze the transient behavior of the CDW intensity on this YBCO cuprate after the optical pump, we first consider when the CDW peaks are changing. According to the CDW works in YBCO [12-14], there are three components to explain how the CDW peaks are changing: 1) Direct perturbation of Cu-charge state (e.g., photo-excited carrier); 2) Sample temperature change (heating); and 3) The known competing effect with SC (only at $T < T_c$ case). These components are respectively represented as blue-, red-, and purple-line in each panel, and the black-colored solid line shows their all summation. Note that each component consists of two exponential functions – decay and recovery with sample amplitude.

For the $T \geq T_c$ case, the temporal intensity change can be analyzed by components 1) and 2), except component 3). It is because the SC effect is not developed. In this case, as shown in Fig. S6a, the CDW firstly undergoes a fast melt near $\Delta t \sim 0$, and then the melted intensity recovers within a few ps time scales. This behavior is mainly explained by component 1). As the fluence increases, we found that the heat effect becomes pronounced with a longer time to recover to initial intensity.

Figure S6b shows an analysis of the temporal CDW intensity change under the superconducting state (i.e., $T < T_c$). It gets somewhat complicated because of the additional SC-related term (i.e., component 3). However, in this case, we could adapt the fitting parameters of components 1) and 2) analyzed at $T \geq T_c$ if the same fluence is used. For $T < T_c$, the overall temporal CDW intensity shows an enhancement because the SC becomes suppressed (Fig. 2). Similar to the case at $T = T_c$ (see Fig. S6a), the higher fluence induces more heat effect and slower the CDW intensity returning. Interestingly, the intensity maximized Δt becomes delayed as the fluence increases, i.e., from ~ 1 ps with $15 \mu\text{J}/\text{cm}^2$ to ~ 3 ps with $60 \mu\text{J}/\text{cm}^2$. We analyze this also comes from the pronounced heat effect in the higher fluence range. In order to minimize

the heat effect during this study, we employed a mild pump fluence $\sim 15 \mu\text{J}/\text{cm}^2$ in the tr-RSXS measurements.

- **X-ray and optical pump penetration depth:** According to CXRO database (The Center for X-Ray Optics at Lawrence Berkeley National Laboratory, <https://www.cxro.lbl.gov/>), the normal incidence penetration depth around Cu L_3 -edge is estimated to be about 120 nm. Considering the sample angle ($\theta = 46^\circ$ for $L = 1.46$) and the detector angle ($2\theta = 167^\circ$), the RSXS probing depth is estimated as ~ 46 nm from the sample surface. According to the previous reports Refs. [35 (L. Stojchevska *et al.*) and 44 (B. Liu *et al.*)], the penetration depth of 800-nm pump laser in $\text{YBa}_2\text{Cu}_3\text{O}_{6+x}$ is estimated as the range of 80-200 nm.

- **X-ray polarization effect in L-dependence of tr-RSXS measurement:** As shown in Fig. 2a, the incident x-ray polarization signal is the π -polarization. Since the CDW intensity is proportional to $\pi \cdot \pi = \cos(2\theta)$, the intensity was rescaled by multiplying $1/\cos(2\theta)$ to compare the intensities in L-dependence.

- **Optical laser polarization effect in tr-RSXS measurement:** In this study, we applied the p -polarized optical pump laser (i.e., $p \parallel bc$ -plane). Since the p -polarized laser has both components along the parallel and orthogonal direction to the CuO_2 plane, a pumping effect in the CuO_2 plane via the p -polarization is effectively weaker than that via the s -polarization ($s \parallel ab$ -plane). As shown in Fig. S7, the optical laser polarization effects were explored. We confirmed that the p -polarization needs more fluence to generate the similar effect shown the s -polarization, especially while the fluence value is high. For the fluence = $15 \mu\text{J}/\text{cm}^2$, which was mainly used in this study, we could find that the difference between two polarizations is minimized.

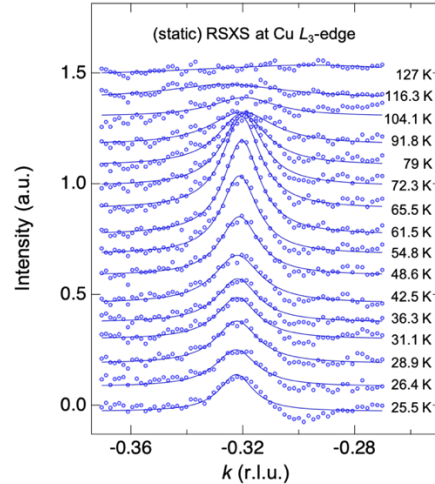


fig. S1. Temperature dependence of the static CDW order in YBCO. The CDW peak observed at $\mathbf{Q} = (0, q_{\text{cdw}}, \sim 1.45)$ where q_{cdw} is around -0.32 reciprocal lattice unit (r.l.u.). The data are subtracted by high temperature (~ 150 K) data. Solid lines are Lorentzian fits to the data.

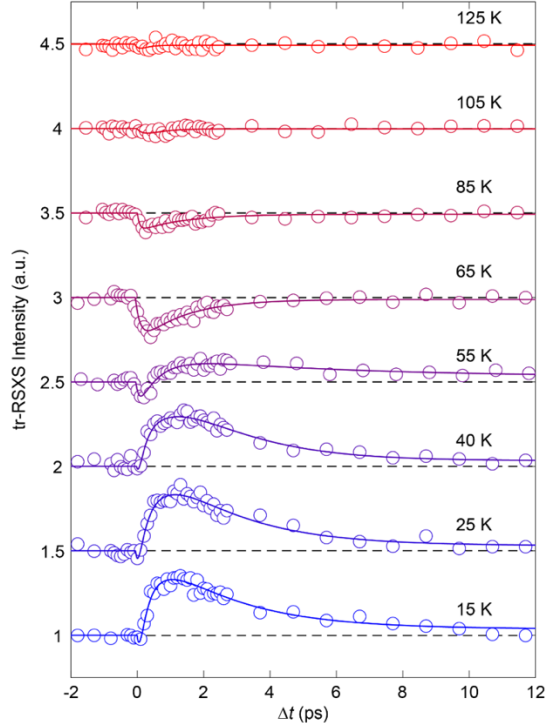


fig. S2. Temporal behavior of the CDW order as a function of temperature. The tr-RSXS intensity was recorded at the CDW at $\mathbf{Q} = (0, -0.32, \sim 1.45)$. Each delay data has been vertically shifted for clarity. The solid line presents fitting by exponential functions. The dashed lines are baselines determined from the negative delay region.

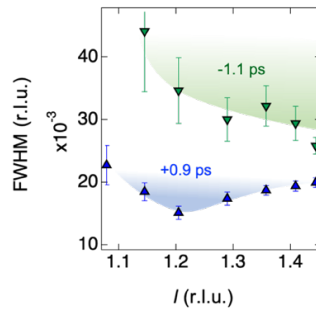


fig. S3. l -dependence of photoinduced CDW. Fitted FWHM of the CDW peaks at l positions (i.e., 2θ) of $\Delta t = +0.9$ ps (up-triangles) and -1.1 ps (down-triangles). Blue and green colored shades are guides-to-the-eye. The error bars represent 1 standard deviation (s.d.) of the fit parameters.

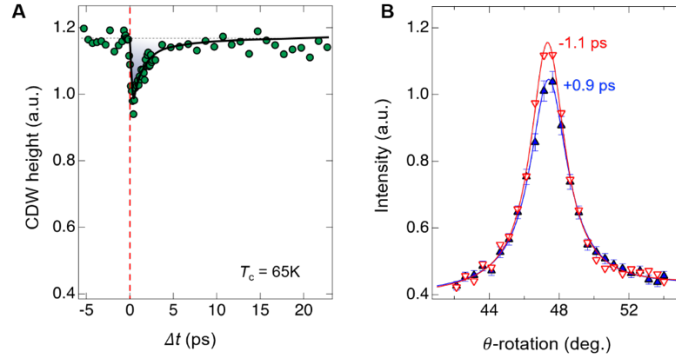


fig. S4. Photoinduced CDW behavior. (A) CDW intensity at $\mathbf{Q} = (0, -0.32, 1.45)$ as a function of Δt , measured at $T = 65$ K ($\sim T_c$). For $\Delta t < 0$, the data indicate the CDW intensity before the pump. For $0 < \Delta t < \sim 5$ ps, the CDW is melted by the optical pump and then is recovered. The maximum melting of CDW occurs at $\Delta t \sim 0.2$ ps. The dashed lines are guides-to-the-eye. (B) The CDW peak profiles at $\Delta t = -1.1$ ps and $\Delta t = +0.9$ ps. At $\Delta t = 0.9$ ps, the CDW intensity recovered to about 83 % of the intensity at $\Delta t < 0$. Solid lines are Lorentzian fits to the data with a linear background.

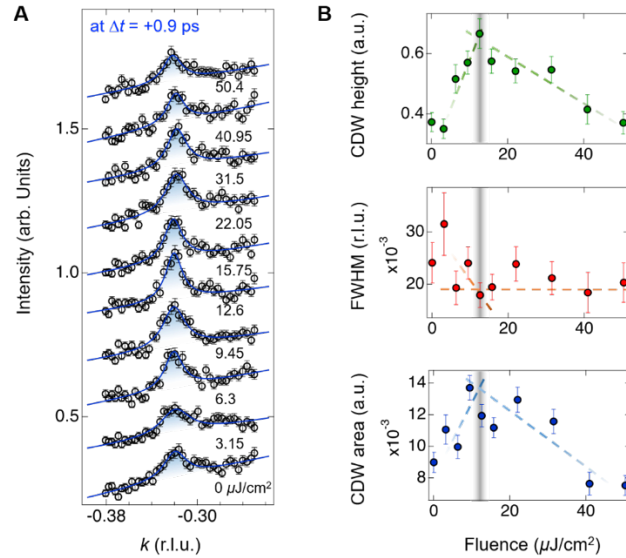


fig. S5. Fluence dependence of photoinduced CDW.(A) CDW intensity at $\mathbf{Q} = (0, -0.32, 1.45)$ with varying laser fluence, measured at $T = 25$ K and $\Delta t = +0.9$ ps. The blue colored lines are Lorentzian fits to the data with a linear background. Each fluence data are vertically shifted by ~ 0.3 arb. Units. (B) Fitted CDW peaks with the different fluence – top: CDW peak's height, middle: FWHM, bottom: integrated intensity (CDW area). The error bars represent 1 standard deviation (s.d.) of the fit parameters. Gray colored shade denotes the employed fluence value in the tr-RSXS. All dashed lines are guides-to-the-eye.

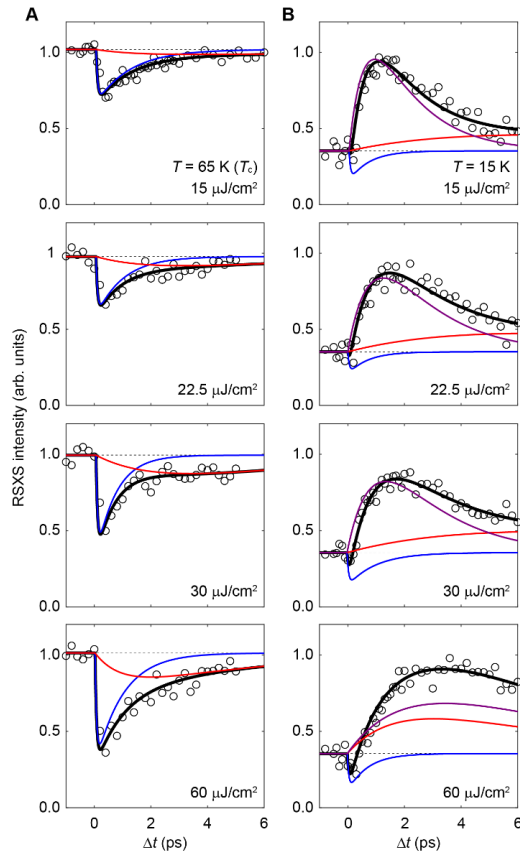


fig. S6. Fluence-dependent delay scans of CDW. Data taken at (0, -0.32, 1.45) and at (A) 65 K (T_c), (B) 15 K. From top to bottom panels, incident fluence increases. Blue, red, and purple lines present fitting of direct perturbation, heating, and SC effect, respectively. Black solid lines show their summation. Black dashed lines display the intensity at $\Delta t < 0$.

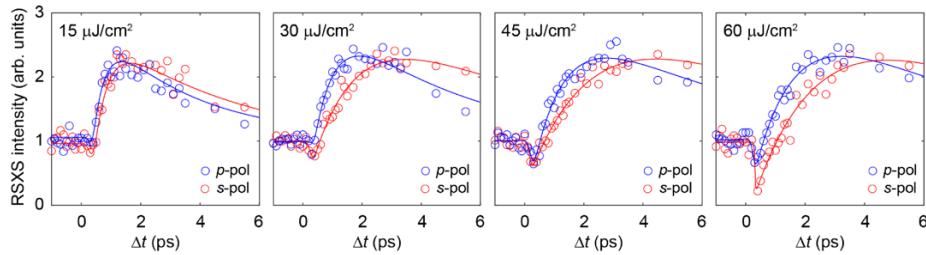


fig. S7. Optical pump laser polarization effect of delay scans of CDW. Data taken at (0, -0.32, 1.45) and 20 K. p -pol (s -pol) is parallel to the crystalline bc (ab)-plane. The solid lines present exponential fitting.

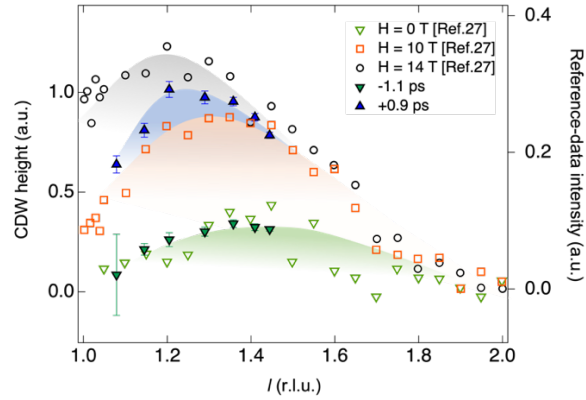


fig. S8. Comparison of L -dependence between the pump-probe and the magnetic field. The magnetic data were taken from the Ref. [27] (Chang *et al.*). To superpose two different data set, we converted x -axis of the reference (x_{ref}) as follow: $l = 2 - x_{\text{ref}}$. Also, it is important to note that the magnetic (H) field data in the reference were measured at $T = 22$ K (this study: $T = 25$ K). Also, the H -field study was measured by the non-resonant hard x-ray scattering (this study by resonant soft x-ray scattering).

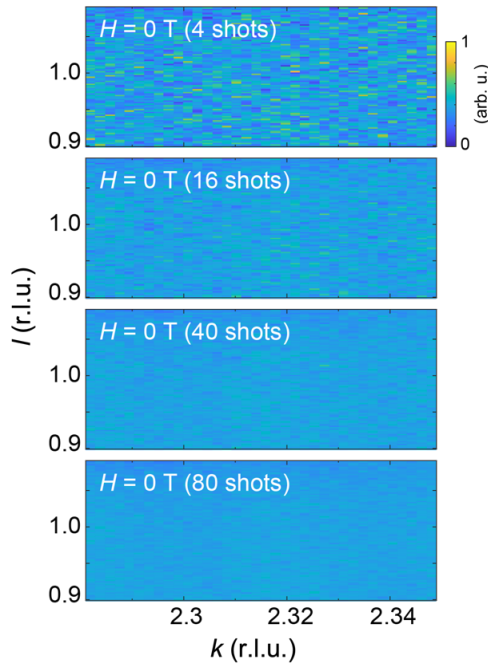


fig. S9. Noise level comparison depending on the number of shots in the magnetic field experiment. All panels show kl -space around $(0, 2+q_{\text{cdw}}, 1)$ under $H = 0$ T. The panels (from top to bottom) are 4-, 16-, 40-, and 80-shots average, respectively. With increasing the shot acquisition, the noise level is reduced.